JOURNAL OF PROPULSION AND POWER
Vol. 24, No. 6, November–December 2008

Dormant Cathode Erosion in a Multiple-Cathode Gridded Ion Thruster

Joshua L. Rovey* and Alec D. Gallimore†
University of Michigan, Ann Arbor, Michigan 48109

DOI: 10.2514/1.37031

A rectangular gridded ion thruster discharge chamber is investigated for operation with multiple discharge cathode assemblies. The multiple-cathode approach attempts to increase thruster throughput and lifetime by operating three discharge cathode assemblies sequentially, possibly providing a threefold increase in discharge chamber life. Previous multiple-cathode electric propulsion devices, such as the SPT-100, have shown dormant-cathode erosion to be a life-limiting phenomenon. Similar results in a multiple-cathode discharge chamber may decrease the anticipated gain in discharge lifetime. To assess possible dormant-cathode sputtering erosion and to determine the operational configuration that minimizes this erosion, diagnostic cylinders are designed and used to measure plasma properties at the dormant-cathode locations. Each diagnostic cylinder appears similar to the active discharge cathode assembly, but is outfitted with Langmuir probes. Plasma properties are then used in a simple sputtering-erosion model to predict erosion of the dormant cathodes. Results indicate that the device should be operated at the 0 A electromagnet current configuration for minimum dormant-cathode erosion. For this optimum configuration, typical number density, electron temperature, and plasma potential values are 5.0×10^{11} cm^{-3}, 5 eV, and 27 V with respect to cathode common, respectively. The erosion model indicates that the dormant cathodes will suffer preoperation erosion, but the erosion rate is 26 times slower than the active discharge cathode assembly. Compared with a single-discharge-cathode-assembly thruster, the model predicts an increase in lifetime by a factor of 2.9 for a triple-discharge-cathode-assembly device.

Nomenclature

A	=	keeper area, m^2
A_p	=	probe area, m^2
E	=	bombarding ion energy, eV
e	=	electron charge, 1.6×10^{-19} C
I_{emag}	=	electromagnet current, A
I_i	=	ion current, A
I_{si}	=	ion saturation current, A
Kn	=	Knudsen number
M_i	=	ion mass, kg
m	=	keeper material mass, kg
n_e	=	electron number density, cm^{-3}
n_i	=	ion number density, cm^{-3}
r	=	probe radius, m
S	=	erosion rate, kg/s
T_e	=	electron temperature, eV
V	=	probe voltage, V
Y	=	sputtering yield, atoms/ion
Γ_i	=	ion flux, cm^{-2} s^{-1}
λ	=	mean free path, m
λ_D	=	Debye length, m
ξ	=	Laframboise dimensionless current correction

I. Introduction

GRIDDED ion thrusters are high-specific-impulse, high-efficiency, advanced space propulsion systems. Three main processes compose gridded ion thruster operation: 1) electron generation, 2) ion production through electron bombardment ionization, and 3) ion extraction using high-voltage grids (ion optics). In modern U.S. ion thrusters, electrons are generated with a hollow cathode called the discharge cathode because it initiates and sustains the plasma discharge. Electrons from the cathode enter the discharge chamber and create ions through electron-bombardment-ionization collisions with neutral atoms, typically xenon. Plasma production is enhanced by increasing the electron path length with a magnetic field. Ions are then extracted and accelerated to significant velocity by high-voltage grids. One prominent example of a contemporary ring-cusp gridded ion thruster is the 30-cm-diam NASA Solar Technology and Application Readiness (NSTAR) ion thruster used on the Deep Space One (DS1) spacecraft. Three NSTAR ion thrusters are in use on the Dawn spacecraft.

Future deep-space missions will require an ion thruster that has long life and the ability to process a large quantity of propellant. In fact, future ion thrusters may be required to operate continuously for as long as 14 years and process greater than 2000 kg of propellant [1–4]. Results from the extended life test (ELT) of the flight spare DS1 NSTAR ion engine show that ion bombardment erosion of the discharge cathode assembly (DCA) limits the operational lifetime of the ion thruster to $\sim$30,000 h [5–7]. Furthermore, wear-test results for the NASA Evolutionary Xenon Thruster (NEXT) DCA show wear profiles similar to the NSTAR thruster [8], suggesting that it may also be limited in life due to ion bombardment erosion. Other DCA failure mechanisms can also occur after prolonged operation. Specifically, depletion of the barium in the insert, brought on by simple barium diffusion and subsequent evaporation, or the formation of tungstates that tie up the barium. Because of such phenomena, a single ion thruster DCA may not be sufficient for missions requiring over 4 years of continuous thruster operation [9].

Methods for extending the ion thruster lifetime have included using more sputter-resistant materials, such as graphite, and developing electrodeless discharge schemes, such as RF and microwave discharges. The Hayabusa spacecraft launched by the Japanese Aerospace Exploration Agency uses microwave-discharge ion thrusters [10]. Another possible approach to increasing thruster throughput and operational lifetime is to use an ion thruster that sequentially operates mulitple DCAs. This approach is more attractive than using multiple ion thrusters because using multiple

Received 6 February 2008; revision received 27 May 2008; accepted for publication 15 June 2008.

*Graduate Student Research Assistant; currently Assistant Professor, Aerospace Engineering, Department of Mechanical and Aerospace Engineering, Missouri University of Science and Technology; roveyj@mst.edu.

†Arthur F. Thurnau Professor, Department of Aerospace Engineering.

cathodes requires less mass. With this approach, a new DCA is ignited when the previous one fails. Ideally, a triple-DCA device will increase the thruster discharge lifetime threefold, making longer mission times a possibility.

The state of the art in multiple-cathode electric propulsion devices consists of two previous research endeavors: a double-cathode ion thruster developed by Hughes Research Laboratories [11] and the stationary plasma thruster SPT-100 [12]. To reduce the bombardment of high-energy ions on a single cathode operated at large discharge currents, the Hughes Research Laboratories developed a discharge chamber containing two hollow cathodes. Operation of the discharge chamber was accomplished with both cathodes operating together at multiple discharge conditions, including low-discharge-current idling and operation with and without beam extraction. However, the cathodes were placed inside a plenum to facilitate uniform electron injection, which caused significant increases in ion production cost. Results from a 5700-h life test of the SPT-100 at the Jet Propulsion Laboratory showed that an operating cathode can cause significant erosion of the nonoperating cathode, thus reducing the overall lifetime [13–15]. The unused cathode actually eroded at the higher rate and collected an order-of-magnitude-higher current density than the active cathode [15]. Even though ion thrusters and SPTs have different geometry and operating characteristics, this is still cause for concern. If the dormant cathodes inside a multiple-cathode ion thruster suffer erosion before being operated, then ion thruster lifetime and throughput may not increase as much as expected.

This paper describes an investigation of the plasma properties near the dormant cathodes in a multiple-cathode discharge chamber (MCDC). Specifically, diagnostic cylinders (DCs) similar in size and shape to the active DCA, but outfitted with plasma diagnostics, are used to measure plasma properties at the dormant-cathode locations inside the MCDC. These plasma measurements, along with a simple sputtering-erosion model, allow us to predict if the dormant cathodes will suffer erosion and how changes in MCDC operation (e.g., magnetic field strength, DCA location, and dormant-cathode electrical connectivity) affect the dormant-cathode erosion rate. The end goal is to determine the mode of MCDC operation that minimizes dormant-cathode erosion and to predict the increase in lifetime provided by a multiple-cathode discharge chamber. The following sections describe the experimental apparatus, data analysis procedure, results, and conclusions.

II. Experimental Apparatus and Setup

A. Vacuum Facility

A large vacuum test facility (LVTF) is used for all experiments. The LVTF is a stainless-steel vacuum chamber with a diameter of 6 m and a length of 9 m. To reach high vacuum, the facility employs seven CVI TM-1200 reentrant cryopumps, each of which is surrounded by an LN_2 baffle. The cryopump system can be operated with any number of pumps in use. For the experiments described here, only two cryopumps were operated, which yielded a base pressure of 5.2×10^{-7} torr. The chamber pressure is monitored using two hot-cathode ionization gauges: an external gauge and a nude gauge. Pressure measurements from the gauges are corrected for xenon using the known base pressure on air and a correction factor of 2.87 for xenon, as described in [16]. Corrected operating pressures for all experiments reported here are below 4.2×10^{-6} torr on xenon.

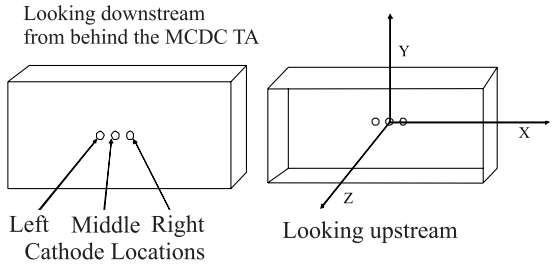

Fig. 1 MCDC coordinate system looking downstream (left) and looking upstream (right).

B. MCDC Test Article

The High Power Electric Propulsion (HiPEP) thruster is a 25-kW, 8000-s specific-impulse ion thruster that is designed to satisfy both the performance and lifetime requirements of the Jupiter Icy Moon Orbiter mission [17]. The MCDC used in this investigation is a rectangular ion thruster discharge chamber based on the HiPEP size and geometry. An electromagnet is placed on the backplate of the MCDC, near the three DCA locations, to adjust the magnetic field. The electromagnet is in addition to the cusped permanent magnet magnetic circuit and allows the magnetic field near the cathodes to be adjusted from approximately 50 to 150 G as the electromagnet current is adjusted from 0 to +10 A. A NEXT-type DCA [18] is mounted to the backplate of the MCDC and used for all experiments. An ion collection grid is mounted at the ion extraction plane because the MCDC is operated as a simulated ion thruster without beam extraction [19]. Attachment of the ion collection grid, the electromagnet, and the NEXT DCA to the MCDC is referred to as the MCDC test article (TA). A schematic of the TA with the chosen coordinate system is shown in Fig. 1. Before data acquisition, the TA is operated for approximately an hour to reach thermal equilibrium, and TA performance parameters are measured to be consistent with previous operational runs.

The general electrical setup of the TA is nearly identical to that described by Brophy [19]; however, in this case, an ion collection grid is used as the ion collection surface instead of high-voltage ion optics. The TA is operated with a 30 A discharge current, cathode common biased +25 V with respect to ground, and a collection grid bias of 20 V below cathode common. For the experiments presented here, ground refers to the vacuum facility potential and cathode common is the cathode potential. In the following experiments, dormant-cathode plasma properties are measured as electromagnet current, DCA location, and DC configuration are adjusted. The DCA is operated at the left, center, and right locations for electromagnet currents of 0, +5, and +10 A. Furthermore, the DCs are operated both electrically connected and electrically isolated (disconnected) from the TA. Table 1 contains the nomenclature for each of these MCDC configurations. Further information regarding the electrical setup and general operation of the TA can be found in [20–22].

Table 1 Nomenclature for the MCDC TA operational configurations investigated

Configuration nomenclature	DCA location	I_{emag}, A	Dormant cathode electrical connectivity
0LC, 0LI	Left	0	Connected, isolated
0MC, 0MI	Center	0	Connected, isolated
0RC, 0RI	Right	0	Connected, isolated
5LC, 5LI	Left	5	Connected, isolated
5MC, 5MI	Center	5	Connected, isolated
5RC, 5RI	Right	5	Connected, isolated
10LC, 10LI	Left	10	Connected, isolated
10MC, 10MI	Center	10	Connected, isolated
10RC, 10RI	Right	10	Connected, isolated

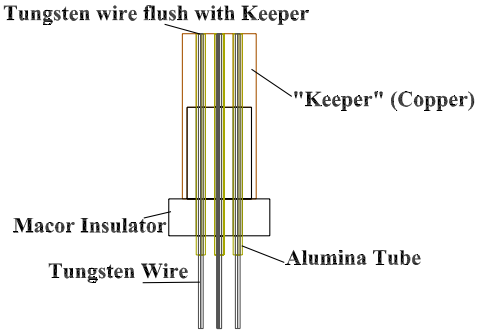

Fig. 2 Schematic of the 5PLP-DC.

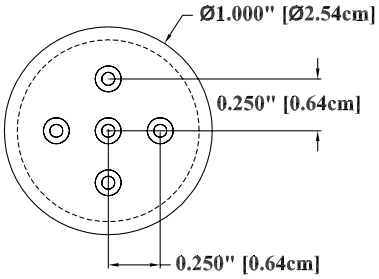

Fig. 3 Probe locations on the 5PLP-DC keeper faceplate.

C. Diagnostic Cylinders

Dormant-cathode plasma properties are measured by designing and implementing DCs that appear similar in size and shape to the active DCA. Commonality in configuration ensures that the TA plasma interacts with the DCs similar to a dormant DCA. Two different DCs are presented in this study: 1) a 5-planar-Langmuir-probe DC (5PLP-DC) and 2) an axial-cylindrical-Langmuir-probe DC (ACLP-DC). Results for a retarding-potential-analyzer DC (RPA-DC) were described in a previous publication and showed that ions accelerate through the dormant-cathode keeper sheath and impact with energy equivalent to the plasma potential [22]. The following sections describe the design, fabrication, and operation of each of the DCs.

1. 5PLP-DC

Two 5PLP-DCs are fabricated to make plasma property measurements at the two dormant-cathode locations internal to the TA. Each DC appears similar to the active DCA; however, each DC keeper electrode is outfitted with 5 planar Langmuir probes (PLPs). A schematic of the 5PLP-DC is shown in Fig. 2 and the 5 PLPs are placed at the spatial locations shown in Fig. 3.

A cylindrical copper keeper is attached to a ceramic insulator to form the base of the DC. The 5PLP-DCs do not contain a cathode electrode. Ten PLPs are constructed of 0.16-cm-diam tungsten wire surrounded by a 0.32-cm-outer-diam alumina tube, yielding a probe area of 2.01 mm^2. Each PLP is inserted axially into the DC such that the probe collecting surface is flush with the keeper faceplate. Five PLPs are placed into each of the two DCs in a symmetrical pattern, with each probe spaced 0.64 cm from the centerline axis. Ceramic epoxy is used to construct the probes and to mate the probes, keeper, and ceramic insulator. Finally, an aluminum mounting flange is used to attach the DC to the TA at one of the dormant-cathode locations.

Electrically, each of the probes is connected to the biasing power supply through a 100-Ω shunt resistor, as shown in Fig. 4. Each probe bias voltage is set with the bias supply, and the corresponding voltage drop across the shunt resistor is measured. Collected current is then calculated by dividing the measured voltage drop by the shunt resistance. In this way, the current-voltage *I-V* characteristic for each probe is determined. Data are acquired for electromagnet currents of 0, +5, and +10 A, with the DC electrically connected and electrically isolated from the TA. During electrically connected operation, the keeper is connected to the anode through a 10-kΩ resistor. As mentioned, the 5PLP-DC does not have a cathode electrode.

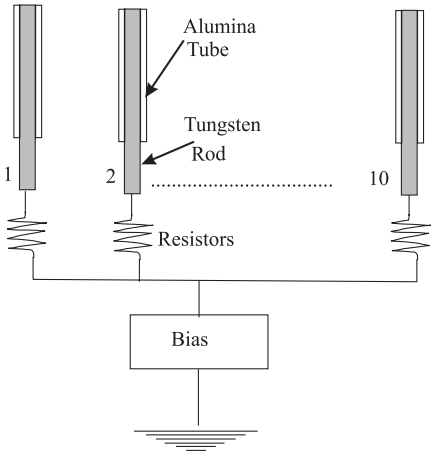

Fig. 4 Electrical schematic of the planar Langmuir probes.

2. ACLP-DC

The ACLP-DC appears similar in size and shape to the active DCA. Concentric cathode and keeper tubes are constructed out of copper and held in place by a ceramic insulator. Keeper and cathode orifice diameters are chosen to be identical to the active DCA. A ceramic insulator is used to hold the keeper and cathode at the required spacing. Two cylindrical Langmuir probes (CLPs) are constructed of 0.25-mm-diam tungsten wire housed in a 1.24-mm-outer-diam alumina tube with the tungsten extending 3.2 mm beyond the tube. This configuration yields a probe area of 2.56 mm^2. Each of the CLPs is 15.2 cm long and is inserted through the DC cathode tube to extend in the positive *Z* axis of the TA. The probe is concentric with the cathode and keeper tubes and is moved axially with respect to the cathode orifice. A 5.1-cm alumina guide tube is inserted in the cathode tube to assist the CLP in passing through the cathode and keeper orifices. This setup allows the probe to be positioned over a 10.2-cm range (7.6 cm external and 2.5 cm internal to the cathode). A schematic of the ACLP-DC is shown in Fig. 5.

Langmuir probe *I-V* characteristics are obtained at various axial locations to determine axial plasma properties at the dormant-cathode positions. The axial probe location is adjusted using a stepper-motor-controlled translation stage mounted with a custom-made probe alignment stand. Data are obtained for both left and middle DCA operation with the electromagnet at 0, +5, and +10 A. ACLP-DC data are not obtained for right DCA operation. The

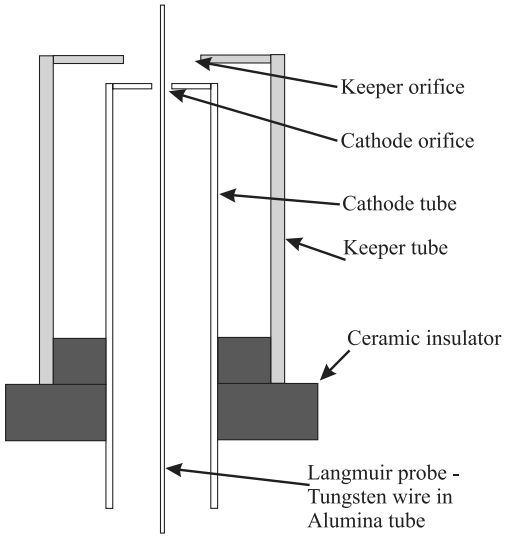

Fig. 5 Schematic of the ACLP-DC.

ACLP-DC is operated both electrically connected and electrically isolated from the TA. During electrically connected operation, the ACLP-DC cathode is connected to cathode common and the keeper is connected to the anode through a 10-kΩ resistor.

III. Analysis Procedure

For the experimental investigation described, both planar and cylindrical single Langmuir probes are used. The following sections describe the data analysis techniques used to analyze the probe data. The standard Knudsen number and Debye length criteria are used to determine when thin-sheath [23] or orbit-motion limited [24] analyses are applied.

A. Thin Sheath

Langmuir probes are typically sized such that the probe operates in the thin-sheath regime. The number density and electron temperature inside the TA are expected to have values within the range of 10^{10}–10^{13} cm^{-3} and 2–10 eV [25], respectively. In the thin-sheath regime, the flux of particles entering the sheath can be calculated without considering the details of the orbits of these particles in the sheath [23]. For a large ratio of probe radius r to Debye length λ_D, the collection area of the probe can be approximated as the area of the probe [23]. A large probe radius helps to minimize edge effects for planar probes (5PLP-DC) and a large ratio of length to radius minimizes the end effects for cylindrical probes (ACLP-DC).

Because there were multiple *I-V* characteristics to analyze, a numerical algorithm is used to analyze the data. A single *I-V* characteristic is used at each point to calculate the plasma parameters. Data files containing *I-V* pairs of data are loaded for each of the probe sweeps and then a thin-sheath data analysis is applied. The electron temperature was calculated as the inverse of the slope of the log-linear *I-V* curve, plasma potential was calculated by finding the maximum in the derivative of the *I-V* curve, and ion saturation current was determined. The measured ion saturation current, electron temperature, and Bohm approximation for ion velocity [26] give the ion number density by the following equation. In this equation, T_e is the electron temperature, e is the elementary charge, A_p is the probe area, I_{si} is the ion saturation current, n_i is the ion number density, and M_i is the ion mass:

$$I_{\text{si}} = 0.61 e n_i \sqrt{\frac{eT_e}{M_i}} A_p \tag{1}$$

B. Orbital Motion Limited

In the orbital-motion limited (OML), or thick-sheath, regime, the sheath dimensions and orbits of particles entering the sheath must be considered. This regime is analyzed by the techniques developed by Laframboise [24] and Laframboise and Parker [27] that assume a cylindrical probe immersed in a cold, collisionless, stationary plasma. In this case, the sheath dimensions are assumed to increase with probe bias such that the collected ion current is affected. Ion current collected by a probe biased below the floating potential is defined by Eq. (2) [24]. In this equation, ξ is a dimensionless current correction developed by Laframboise [24] that depends on probe size, plasma number density, and temperature. For the temperatures and number densities obtained in most ion thruster plasma, Steinbrüchel [28] suggested that ξ is given to within 3% error by Eq. (3):

$$I_i = \xi e n_i \sqrt{\frac{eT_e}{2\pi M_i}} A_p \tag{2}$$

$$\xi = \sqrt{\frac{1.27V}{T_e}} \tag{3}$$

Combining Eqs. (2) and (3) allows I^2 to be plotted as a linear function of V, and the ion number density can then be calculated as a function of the slope of I^2 versus V, as illustrated in Eq. (4). In this equation, n_i is the ion number density, A_p is the probe area, I_i is the ion current, V is the probe voltage, M_i is the ion mass, and e is the elementary charge:

$$n_i = \frac{1}{A_p} \sqrt{\frac{\mathrm{d}I_i^2}{\mathrm{d}V} \frac{2\pi M_i}{1.27 e^3}} \tag{4}$$

Chen [29] suggested that the OML regime is entered when the ratio of probe radius to Debye length is less than approximately 3. Because only the number density calculation changes in this OML analysis, the preceding thin-sheath analysis is augmented to contain an OML option. The thin-sheath analysis is initially blindly applied; however, if the Debye length is calculated to be less than one-third of the probe radius, then the OML number density calculation is used. An OML calculation is unnecessary for a planar probe [27], and so only the ACLP-DC results are subjected to the OML subroutine option. More discussion about the ACLP-DC axial locations over which OML is necessary can be found in the following sections.

C. Magnetic Field Effects

The presence of a magnetic field can alter the *I-V* characteristic obtained by a single Langmuir probe. The electron retarding region used to determine the electron temperature is generally not affected, but the electron saturation current is affected [30,31]. Because electrons spiral around magnetic field lines, if the cyclotron radius of electrons is of the same magnitude as the probe radius, then probe sheath structures can become nonsymmetric or oblong, causing the electron saturation current of the probe trace to be reduced. As magnetic field strength increases, the electron saturation current decreases, because spiraling electrons are unable to cross the magnetic field lines and become collected by the probe [30,31]. However, the analysis presented here obtains the number density from the ion saturation current, and the magnetic field in the bulk discharge region of the MCDC is not large enough to have an appreciable effect on ion collection. Even in the cusp regions of the MCDC in which the magnetic field can be on the order of 1000 G, the ion cyclotron radius is an order of magnitude larger than the radius of the probe. Therefore, the presence of the magnetic field is not expected to affect the number density measurement.

Because the electron saturation current is reduced due to the presence of a magnetic field, the resulting plasma potential, which is typically determined from the knee of the electron retarding region (or the maximum of the first derivative), is affected. Specifically, the magnetic field causes the calculated plasma potential to be less than its true value. This shift can be accounted for and is dependent on the orientation of the probe with respect to the magnetic field, the electron temperature, and the mean free path of electrons [31]. However, for the results presented here, the shift of the plasma potential due to the magnetic field (less than 1*V*) [31] is less than the error associated with the calculation of plasma potential from the single Langmuir probe data. Therefore, the effect of the magnetic field is not considered in the analysis algorithm.

D. Error Analysis

Traditional error estimates for electrostatic single Langmuir probes are typically 50 and 20% for number density and electron temperature, respectively [32]. However, the relative error between measurements using the same experimental setup is expected to be considerably smaller. Using methods similar to those presented here, Foster [33] estimated the overall uncertainties in Langmuir probe measurements and found 15 and 25% for electron temperature and number density, respectively. The uncertainty in the number density is determined by the sum of the fractional uncertainty in the ion current (15%) and the fractional uncertainty in the square root of the electron temperature (7.5%). Data acquired after venting and then evacuating the facility showed agreement to within 5%.

IV. Results

A. 5PLP-DC

The following section describes the results obtained using the 5PLP DCs for left, middle, and right DCA TA operation. Results are shown from the perspective of a viewer looking downstream from behind the TA, following the coordinate system in Fig. 1. In the following figures, three different TA configurations are shown, and for each configuration, the three large circles represent the three cathodes: one active cathode (DCA) and two DCs. Each dot inside the circles represents one of the PLPs. The configuration nomenclature in each figure is described in Table 1. All voltages are referenced with respect to cathode common. In general, the connectivity of the DC had no effect on plasma properties.

Typical measured floating voltages are between 2–14 V above cathode potential with floating voltage increasing with electromagnet current. For the 0 A electromagnet current configuration, floating voltages are, on average, 5 V above cathode potential. Results suggest that DCA active location and floating potential are uncorrelated. Measured electron temperatures are typically within 3–6 eV, with electron temperature decreasing with increasing electromagnet current. The 0 A electromagnet configuration (as shown in Fig. 6) shows electron temperatures between 4–6 eV. Right and middle DCA configurations show higher electron temperatures on the left side of the TA, and this difference decreases with increasing electromagnet current.

Plasma potentials are measured to be 27–33 V, with plasma potential increasing with increasing electromagnet current. The 0 A electromagnet current condition (Fig. 7) shows plasma potentials approximately 2–5 V above the discharge voltage of ∼24.5 V. Measured plasma potential is typically higher for the right DCA active configurations. Figure 8 shows that measured number densities were between 8.9×10^{10} and 2.5×10^{11} cm^{-3}, with number density decreasing with increasing electromagnet current. For the 0 A configuration, number densities are consistently 1.3×10^{11} to 2.5×10^{11} cm^{-3} .

B. ACLP-DC

The ACLP-DC is used for left active and middle active DCAs. Typical raw data *I-V* characteristics are shown in Fig. 9. When the probe is external to the DC (positive axial positions), the *I-V* characteristic appears as expected. As the probe moves internal to the DC (negative axial positions), the collected current significantly decreases, leading to an almost linear *I-V* characteristic with a small slope. The decrease in probe signal leads to a smaller signal-to-noise ratio, and as a result, the probe analysis procedure is unable to calculate the plasma parameters for some spatial locations. Specifically, internal to the DC, *I-V* characteristic derivatives become quite noisy and the log-linear current versus voltage plot can no longer be used to obtain the electron temperature.

Figure 10 shows the axial plasma properties for the ACLP-DC. All voltages are referenced with respect to cathode common. An axial position of zero on the plots corresponds to the external side of the cathode orifice, and positions are measured from the tungsten-wire–alumina-sleeve interface on the probe. Because the probe is cylindrical, certainty in axial position is compromised and determined to be the length of the probe electrode (∼3 mm). Number density decreases as the probe moves internal to the DC, and so an OML analysis becomes important. Transition to the OML regime is determined to occur at ∼3 mm internal to the DC. At this location, the thin-sheath number density calculation is aborted and an OML calculation is implemented. Again, DC connectivity has no noticeable effect on plasma properties.

As the probe moves internal to the DC, Fig. 10 shows that plasma density decreases 2 orders of magnitude in 5 mm, and by 20 mm, the ion current has become undetectable. At ∼3 mm internal to the DC, an OML analysis is substituted for the thin-sheath analysis. As a result of the decreased density, the signal-to-noise ratio of the probe trace decreases and the *I-V* characteristic becomes more difficult, and sometimes impossible, to analyze. This causes the data points

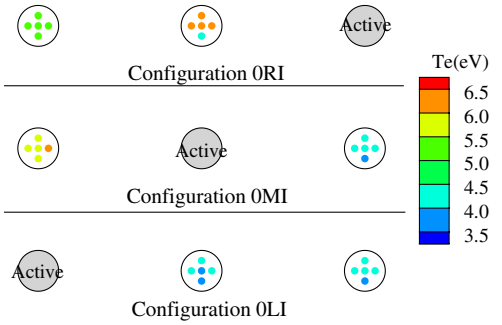

Fig. 6 The 5PLP-DC electron temperature results for the 0RI, 0MI, and 0LI TA configurations.

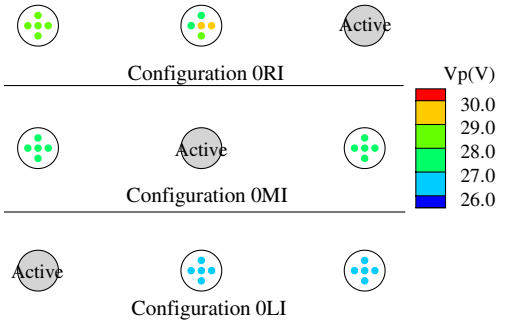

Fig. 7 The 5PLP-DC plasma potential results for the 0RI, 0MI, and 0LI TA configurations.

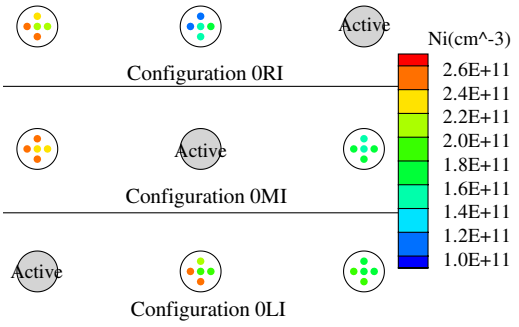

Fig. 8 The 5PLP-DC number density results for the 0RI, 0MI, and 0LI TA configurations.

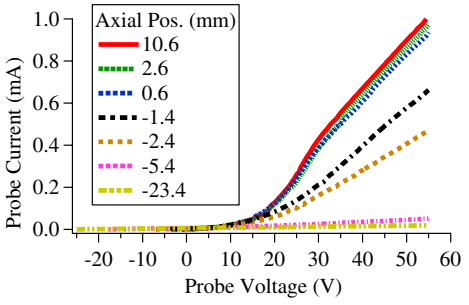

Fig. 9 Typical ACLP-DC raw data *I-V* characteristics as a function of axial position; as the probe moves inside the DC, the probe current significantly decreases.

internal to the DC to exhibit more noise, and this is evident in the electron temperature and plasma potential plots of Fig. 10.

External number density is on the order of 5.0×10^{11} cm^{-3}. As electromagnet current increases, external number density decreases. Plasma potential values external to the DC are typically on the order

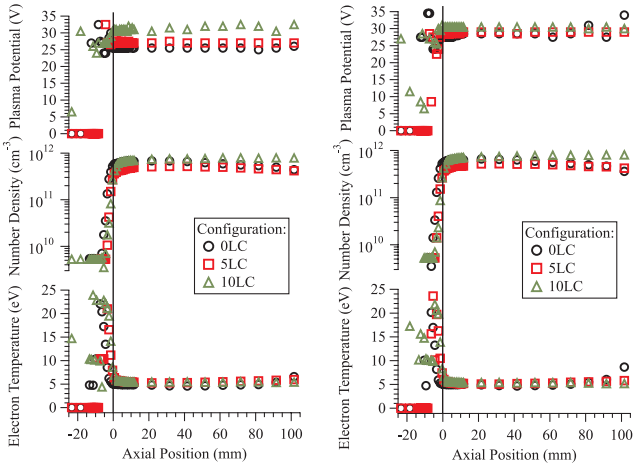

Fig. 10 ACLP-DC plasma property axial profiles for the right DC for the investigated TA operational configurations for the DCA at the a) middle and b) right locations.

of 26–30 V above cathode potential (2–4 V above the discharge voltage), and plasma potential increases with electromagnet current. Internal to the DC plasma potential shows a slight decrease of approximately 40%. The external electron temperature is typically 3–5 eV. As the probe moves internal to the DC, electron temperature increases. Specifically, electron temperature increases by a factor of 5. This result suggests that only the most energetic electrons are capable of entering the DC. Floating-potential measurements are within the expected range of 3–12 V external to the DC. As the probe moves internal to the DC, floating potential drops to −25 V with respect to cathode common (i.e., ground). This result is explained by the measured increase in electron temperature internal to the DC. A lower floating potential is required to repel the higher-temperature electrons inside the DC. This drop in floating potential occurs over a shorter length scale (10 mm) for the 5- and 10 A electromagnet settings, but requires approximately 25 mm of length for the 0 A electromagnet current setting.

Internal and external axial plasma properties were measured by Goebel et al. [34] for the NSTAR DCA. Comparison of the results in Fig. 10 for a dormant cathode with those obtained by Goebel et al. for an active DCA showed marked differences. Active-DCA results showed a peak number density of 1×10^{15} cm^{-3} at the DCA orifice that decreased to 1×10^{12} cm^{-3} within 6 cm downstream (external) and to 2×10^{13} cm^{-3} within 1 cm upstream (internal). Further, plasma potential at the keeper orifice was 12 to 14 V for the active DCA, and this value increased to 17 V within 2 cm external to the DCA and decreased to 6 V internal to the DCA. Finally, the electron temperature for the active DCA was 2 eV at the keeper orifice, and this value increased to 4 eV at 2 cm downstream and decreased to 1 eV internal to the DCA. Goebel et al. were able to obtain cleaner results and clearer trends internal to the active DCA because the plasma density was significantly larger than the internal dormant cathodes presented here. The differences in these results are expected because the active DCA is producing plasma and sustaining the thruster discharge, whereas the dormant cathodes are simply immersed in the discharge plasma.

The most important result from the data shown in Fig. 10 is the existence of relatively uniform plasma external to the dormant cathodes. Measurements of plasma properties near an active DCA by Gallimore et al. [35] showed that the plasma potential varies significantly (∼10–15 V) and causes acceleration of ions that bombard the DCA keeper. Specifically, the near-DCA plasma potential sets up a potential structure that attracts and focuses ions into the DCA, causing the known wear patterns and erosion. The absence of this structure at the dormant-cathode locations is fortunate because only those ions that randomly drift across the dormant-cathode keeper sheath will impact the keeper and cause sputtering erosion. Ions will not be pulled and focused into the dormant cathodes like they are at the active DCA. So the number of ions damaging the dormant cathodes will be less than the active DCA, and we can conclude that the preoperation erosion rate of the dormant cathodes will be less than the erosion rate of the active DCA. Therefore, a MCDC is expected to increase the lifetime of an ion thruster.

V. Discussion

The dominant wear mechanism for the active DCA is known to be sputtering erosion caused by plasma ions that bombard the DCA [35]. This form of wear is also present for the dormant cathodes. The erosion rate will be determined by both the energy and quantity of impinging ions. In its simplest form, the erosion rate S (kg/s) can be expressed by Eq. (5), in which Γ_i is the flux of ions to the cathode surface (ions/m$^2 \cdot$ s), A is the area being bombarded (m^2), m is the mass of the keeper material (kg/atom), and $Y(E)$ is the sputtering yield (atoms/ion) as a function of the bombarding ion energy E:

$$S = \Gamma_i A m Y(E) \tag{5}$$

Results indicate a relatively flat plasma distribution near the dormant cathodes, and so we assume a random flux of ions to the dormant-cathode sheath that is directly proportional to the ion number density. Furthermore, Doerner et al. [36] measured the sputtering yield dependence on bombarding ion energy for normal-incidence xenon on molybdenum, the NSTAR DCA material. In this model, we assume that an ion will gain the plasma potential energy as it falls through the dormant-cathode sheath. This assumption is in agreement with previous dormant-cathode ion energy measurements [22]. Therefore, the erosion rate is dependent on both the number density and plasma potential. Of the independent variables investigated (i.e., magnetic field, DCA configuration, and DCA location), our results show that the magnetic field is the only variable that can be used to alter the plasma properties and hence the preoperation erosion. DCA active location is irrelevant for this analysis because all three DCAs must be operated in a flight device and DC connectivity did not affect the plasma properties.

The two extreme magnetic field configurations were the 0- and +10-A electromagnet currents, which yielded average number densities of 5.0×10^{11} and 2.0×10^{11} cm^{-3} and plasma potentials of 27 and 35 V, respectively. These plasma potential energies correspond to sputtering yields of 1.8×10^{-4} and 7.4×10^{-4} atoms/ion, respectively, for singly charged ions based on the Doerner et al. [36] data for normal ion incidence. So, regardless of the operating condition, the dormant cathodes will suffer preoperation erosion. Assuming an equivalent area, molybdenum keeper material, and ion temperature (thermal velocity), the ratio of the erosion rates for the 0- to +10-A electromagnet current configurations is 0.67; the 0 A current configuration will suffer approximately 33%, or one-third, less preoperation erosion. The 0 A electromagnet current appears to be the MCDC TA operational configuration that minimizes dormant-cathode erosion.

Next, we compare the dormant-cathode and active-DCA erosion rates. During previous wear tests, the maximum measured erosion rate for the active DCA was 70 μm/kh [5,6]. In this model, we assume the erosion is uniform across the face of the DCA keeper and a modest 50 μm/kh, based on previous wear-test erosion measurements [5,6]. The ion temperature near the active DCA has been measured to be 0.5–1.5 eV [37]. We assume a value of 1.0 eV for the random-flux calculation. The area and material of both the active and dormant devices are equivalent. For singly charged ions only, the analysis indicates that the active DCA erodes 26 times faster than the dormant cathode. This difference is attributable to the absence of a focusing plasma structure at the dormant-cathode location, which led to our random-flux assumption. If doubly charged ions are taken into account, assuming a 20% doubles-to-singles ratio based on downstream plume measurements [38], then the active DCA erodes 9 times faster than the dormant cathode. This

difference is attributable to the increased bombarding energy that a doubly charged ion gains as it falls through the plasma potential.

Finally, we can calculate a predicted lifetime increase of a triple-DCA MCDC by using the calculated erosion rates. We assume that an active DCA is terminated after the keeper face plate is entirely eroded away. During operation of the first DCA, the two dormant units suffer preoperation erosion at a rate 26 and 9 times less than the active device for singly-charged-only and doubles-included analyses, respectively. Using this assumption, for singly charged only, the analysis indicates that the first, second, and third DCAs will operate for 30,233, 29,092, and 27,995 h, respectively. This provides a factor-of-2.9 increase in the lifetime over a single DCA device. When doubly charged ions are included, the analysis indicates that the first, second, and third DCAs will operate for 30,233, 26,813, and 23,780 h, respectively. The gain in lifetime is then a factor of 2.7 over the single DCA device.

VI. Conclusions

Dormant-cathode plasma properties are analyzed using DCs designed to appear similar to the active DCA. Each DC is equipped with Langmuir probes. Two different DCs are used: 5PLP-DC and ACLP-DC. Each DC is mounted at a dormant-cathode location in the MCDC TA. Results show no variation in plasma properties between operating the dormant cathodes electrically connected (cathode connected to cathode common and keeper connected to the anode through a 10-$k\Omega$ resistor) or electrically isolated (both cathode and keeper floating) from the TA. As the electromagnet current increases, the backplate magnetic field increases, causing the near dormant-cathode electron temperature and number density to decrease, whereas the plasma potential increases. Furthermore, the typical external number density of $\sim 5.0 \times 10^{11}$ cm^{-3} falls off 2 orders of magnitude within 5 mm internal to the dormant cathodes, and data obtained internal to the DCs are more difficult to analyze, due to a decreased signal-to-noise ratio.

For the 0 A electromagnet configuration typical number density, electron temperature, and plasma potential values are on the order of 5.0×10^{11} cm^{-3}, 5 eV, and 27 V with respect to cathode common, respectively. Plasma potentials are typically 2–4 V above the discharge voltage, which is nominally 24.5 V. As electromagnet current increases from 0 to 10 A, plasma potential increases from 27 to 35 V, electron temperature decreases from 5 to 3 eV, and number density decreases from 5.0×10^{11} to 2.0×10^{11} cm^{-3}.

A simple erosion model indicates that the dormant cathodes suffer preoperation erosion. However, the erosion rate is expected to be a factor of 26 less for singly charged only and a factor of 9 less when doubly charged ions are included. Furthermore, a simple erosion model calculation shows that the operating configuration that yields minimum dormant-cathode erosion has 0 A electromagnet current. The 0 A electromagnet current configuration is a compromise between bombarding ion flux (ion number density) and energy (plasma potential) to yield the lowest erosion rate. Based on these results, a MCDC device is expected to increase the ion thruster lifetime. However, based on the calculated erosion rates, a triple-DCA MCDC will not increase the lifetime by a factor of 3, due to preoperation erosion of the dormant cathodes. Instead, the lifetime is anticipated to increase by a factor of 2.9 if only singly charged ions bombard the cathodes. When doubly charged ions are included, the lifetime increase is a factor of 2.7.

Acknowledgments

We would like to thank Michael Patterson of NASA John H. Glenn Research Center (GRC) at Lewis Field for the financial support of this research through research grant NNC04GA67G and for the use of government-furnished equipment. We would like to acknowledge John Foster (grant monitor) who was the principal contact at NASA GRC. Joshua Rovey was additionally supported through a Michigan Space Grant Consortium graduate fellowship. This support is gratefully acknowledged. We would also like to thank the entire research group at the Plasmadynamics and Electric Propulsion Laboratory (PEPL), who were instrumental in this investigation, including Terry Larrow for fabricating the hardware used in this study and Ryan Kurkul for experimental setup and data acquisition assistance.

References

[1] Patterson, M. J., Roman, R. F., and Foster, J. E., "Ion Engine Development for Interstellar Precursor Missions," 36th AIAA Joint Propulsion Conference, AIAA Paper 2000-3811, Huntsville, AL, July 2000.

[2] Oleson, S., "Electric Propulsion Technology Development for the Jupiter Icy Moon Orbiter Project," 40th AIAA Joint Propulsion Conference, AIAA Paper 2004-3449, Fort Lauderdale, FL, July 2004.

[3] Rawlin, V. K., Williams, G. J., Pinero, L., and Roman, R. F., "Status of Ion Engine Development for High Power, High Specific Impulse Missions," 27th International Electric Propulsion Conference, International Electric Propulsion Conference Paper 01-096, Pasadena, CA, Oct. 2001.

[4] Randolph, T., and Polk, J. E., "An Overview of the Nuclear Electric Xenon Ion System (NEXIS) Activity," 40th AIAA Joint Propulsion Conference, AIAA Paper 2004-3450, Fort Lauderdale, FL, July 2004.

[5] Sengupta, A., Brophy, J. R., Anderson, J. R., Garner, C. E., de Groh, K., et al., "An Overview of the Results from the 30,000 Hr Life Test of Deep Space 1 Flight Spare Ion Engine," 40th AIAA Joint Propulsion Conference, AIAA Paper 2004-3608, Fort Lauderdale, FL, July 2004.

[6] Sengupta, A., Brophy, J. R., and Goodfellow, K., "Status of the Extended Life Test of the Deep Space 1 Flight Spare Engine After 30,352 Hours of Operation," 39th AIAA Joint Propulsion Conference, AIAA Paper 2003-4558, Huntsville, AL, July 2003.

[7] Sengupta, A., "Destructive Physical Analysis of Hollow Cathodes from the Deep Space 1 Flight Spare Ion Engine 30,000 Hr Life Test," 29th International Electric Propulsion Conference, International Electric Propulsion Conference Paper 2005-026, Princeton, NJ, 2005.

[8] Kamhawi, H., Soulas, G. C., Patterson, M. J., and Frandina, M. M., "NEXT Ion Engine 2000 Hr Wear Test Plume and Erosion Results," 40th AIAA Joint Propulsion Conference, AIAA Paper 2004-3792, Fort Lauderdale, FL, July 2004.

[9] Kovaleski, S. D., Patterson, M. J., Soulas, G. C., and Verhey, T. R., "A Review of Hollow Cathode Testing for the International Space Station Plasma Contactor," 27th International Electric Propulsion Conference, International Electric Propulsion Conference Paper 01-271, Pasadena, CA, Oct. 2001.

[10] Kuninaka, H., Nishiyama, K., Shimizu, Y., Hosoda, S., Koizumi, H., et al., "Status of Microwave Discharge Ion Engines on Hayabusa Spacecraft," 43rd AIAA Joint Propulsion Conference, AIAA Paper 2007-5196, Cincinnati, OH, July 2007.

[11] Poeschel, R. L., "Development of Advanced Inert-Gas Ion Thrusters," Hughes Research Labs., Rept. NAS3-22474, Malibu, CA, June 1983.

[12] King, L. B., "Transport-Property and Mass Spectral Measurements in the Plasma Exhaust Plume of a Hall Effect Space Propulsion System," Ph.D. Thesis, Dept. of Aerospace Engineering, Univ. of Michigan, Ann Arbor, MI, 1998.

[13] Garner, C. E., Brophy, J. R., Polk, J. E., and Pless, L. C., "Cyclic Endurance Test of a SPT-100 Stationary Plasma thruster," 30th AIAA Joint Propulsion Conference, AIAA Paper 94-2856, Indianapolis, IN, June 1994.

[14] Garner, C. E., Brophy, J. R., Polk, J. E., and Pless, L. C., "A 5,730 Hr Cyclic Endurance Test of the SPT-100," 31st AIAA Joint Propulsion Conference, AIAA Paper 95-2667, San Diego, CA, July 1995.

[15] Day, M., Kim, V., Kozlov, V. I., Popov, G. A., and Skrylnikov, A. I., "Investigation of the nonoperating cathode erosion reasons," 32nd AIAA Joint Propulsion Conference, AIAA Paper 96-2710, Lake Buena Vista, FL, July 1996.

[16] Dushman, S., *Scientific Foundations of Vacuum Technique*, Vol. 4, Wiley, New York, 1958.

[17] Foster, J. E., Haag, T. W., Kamhawi, H., Patterson, M. J., Malone, S., et al., "The High Power Electric Propulsion Thruster," 40th AIAA Joint Propulsion Conference, AIAA Paper 2004-3812, Fort Lauderdale, FL, July 2004.

[18] Patterson, M. J., Foster, J. E., Haag, T. W., Rawlin, V. K., and Soulas, G. C., "NEXT: NASA's Evolutionary Xenon Thruster," 38th AIAA Joint Propulsion Conference, AIAA Paper AIAA 2002-3832, Indianapolis, IN, July 2002.

[19] Brophy, J. R., "Simulated Ion Thruster Operation Without Beam Extraction," 21st International Electric Propulsion Conference, AIAA Paper 90-2655, Orlando, FL, July 1990.

[20] Rovey, J. L., and Gallimore, A. D., "Performance and Flatness of a Multiple-Cathode, Rectangular Ion Thruster Discharge Chamber," *Journal of Propulsion and Power*, Vol. 23, No. 1, Jan.–Feb. 2007, pp. 44–50.
doi:10.2514/1.21325

[21] Rovey, J. L., "A Multiple-Cathode, High-Power, Rectangular Ion Thruster Discharge Chamber for Increasing Thruster Lifetime," Ph.D. Thesis, Dept. of Aerospace Engineering, Univ. of Michigan, Ann Arbor, MI, 2006.

[22] Rovey, J. L., and Gallimore, A. D., "Ion Energy Measurements Near a Dormant Cathode in a Multiple-Cathode Gridded Ion Thruster," *Physics of Plasmas*, Vol. 14, No. 3, Mar. 2007, pp. 03305-1–03305-8.

[23] Mott-Smith, H. M., and Langmuir, I., "The Theory of Collectors in Gaseous Discharges," *Physical Review*, Vol. 28, Oct. 1926, pp. 727–763.
doi:10.1103/PhysRev.28.727

[24] Laframboise, J. G., "Theory of Spherical and Cylindrical Langmuir probes in a Collisionless, Maxwellian Plasma at Rest," Univ. of Toronto, Inst. for Aerospace Studies, Rept. 100, Toronto, June 1966.

[25] Herman, D. A., "The Use of Electrostatic Probes to Characterize the Discharge Plasma Structure and Identify Discharge Cathode Erosion Mechanisms in Ring-Cusp Ion Thrusters," Ph.D. Thesis, Dept. of Aerospace Engineering, Univ. of Michigan, Ann Arbor, MI, 2005.

[26] Chen, F. F., *Introduction to Plasma Physics and Controlled Fusion*, Plasma Physics, Vol. 1, Plenum, New York, 1984.

[27] Laframboise, J. G., and Parker, L. W., "Probe Design for Orbit-Limited Current Collection," *Physics of Fluids*, Vol. 16, No. 5, May 1973, pp. 629–636.
doi:10.1063/1.1694398

[28] Steinbrüchel, C., "Langmuir Probe Measurements on CHF_3 and CF_4 Plasmas: The Role of Ions in the Reactive Sputter Etching of SiO_2 and Si," *Journal of the Electrochemical Society*, Vol. 130, No. 3, Mar. 1983, pp. 648–655.
doi:10.1149/1.2119774

[29] Chen, F. F., "Electric Probes," *Plasma Diagnostic Techniques*, edited by R. H. Huddlestone, and S. L. Leonard, Academic Press, New York, 1965.

[30] Brown, I. G., Compher, A. B., Kunkel, W. B., "Response of a Langmuir Probe in a Strong Magnetic Field," *Physics of Fluids*, Vol. 14, No. 7, July 1971, pp. 1377–1383.
doi:10.1063/1.1693617

[31] Sugawara, M., "Electron Probe Current in a Magnetized Plasma," *Physics of Fluids*, Vol. 9, No. 4, Apr. 1966, pp. 797–800.
doi:10.1063/1.1761746

[32] Hutchinson, I. H., *Principles of Plasma Diagnostics*, 2nd ed., Cambridge Univ. Press, Cambridge, England, U.K., 2002.

[33] Foster, J. E., "Intercusp Electron Transport in an NSTAR-Derivative Ion thruster," *Journal of Propulsion and Power*, Vol. 18, No. 1, Jan. 2002, pp. 213–217.

[34] Goebel, D. M., Jameson, K. K., Katz, I., and Mikellides, I., "Energetic Ion Production and Keeper Erosion in Hollow Cathode Discharges," 29th International Electric Propulsion Conference, International Electric Propulsion Conference Paper 2005-266, Princeton, NJ, 2005.

[35] Gallimore, A. D., Rovey, J. L., and Herman, D. A., "Erosion Processes of the Discharge Cathode Assembly of Ring-Cusp Gridded Ion Thrusters," *Journal of Propulsion and Power*, Vol. 23, No. 6, Nov.–Dec. 2007, pp. 1271–1278.
doi:10.2514/1.27897

[36] Doerner, R. P., Whyte, D. G., and Goebel, D. M., "Sputtering Yield Measurements During Low Energy Xenon Plasma Bombardment," *Journal of Applied Physics*, Vol. 93, No. 9, May 2003, pp. 5816–5823.
doi:10.1063/1.1566474

[37] Williams, G. J., Smith, T. B., Domonkos, M. T., Gallimore, A. D., and Drake, R. P., "Laser-Induced Fluorescence Characterization of Ions Emitted from Hollow Cathodes," *IEEE Transactions on Plasma Science*, Vol. 28, No. 5, Oct. 2000, pp. 1664–1675.
doi:10.1109/27.901252

[38] Williams, G. J., Domonkos, M. T., and Chavez, J. M., "Measurement of Doubly Charged Ions in Ion Thruster Plumes," 27th International Electric Propulsion Conference, International Electric Propulsion Conference Paper 01-310, Pasadena, CA, Oct. 2001.

R. Myers
Associate Editor